Raman Difference Spectroscopic Studies of the Myosin S1·MgADP·Vanadate Complex†

Hua Deng,§ Jianghua Wang,‡ Robert H. Callender,*,§ Jean C. Grammer,|| and Ralph G. Yount||

Department of Physics, City College of the City University of New York, New York, New York 10031, Department of Biochemistry, Albert Einstein College of Medicine, Bronx, New York 10461, and Department of Biochemistry and Biophysics, Washington State University, Pullman, Washington 99164

Received March 11, 1998; Revised Manuscript Received May 20, 1998

ABSTRACT: The Raman spectra of the nonbridging V⋯O bonds in the myosin S1·MgADP·Vi complex, often believed to be a transition-state analogue for the phosphotransfer reaction catalyzed by myosin, and in a vanadate solution model compound have been obtained using Raman difference spectroscopic techniques. A symmetric/asymmetric pair of modes at 870 cm^{-1} is found for vanadate in solution while three bands are found in the myosin S1·MgADP·Vi complex at 870, 844, and 829 cm^{-1}. Using empirical relationships that relate bond order/bond lengths to stretch frequencies, the bond order and bond length of the three nonbridging V⋯O bonds of vanadate in solution were determined to be 1.43 vu (±0.04 vu) and 1.669 Å (±0.004 Å), respectively. The average bond order and bond length of the nonbridging V⋯O bonds in the S1·MgADP·Vi complex were determined to be 1.38 vu and 1.683 Å. A normal-mode analysis suggests that the VO_3^{2-} moiety approaches a planar conformation in the enzymic complex. Ab initio calculations show that a water molecule at the S1 ATPase binding site, in line with the apical O−V bond in the ADP−Vi moiety and believed to be the attacking nucleophile in the phosphotransfer reaction, can account well for the changes in frequencies of vanadate when it binds to the protein by forming a moderately strong V−O(H_2) bond. Hence, an important role determining the ATPase activity at the active site of myosin appears to be a strategic positioning of this in-line water molecule. Assuming that the distortions that vanadate undergoes upon forming the S1·MgADP·Vi complex are analogous to the changes of the γ-phosphate of ATP in the transition state of the myosin-catalyzed hydrolysis, our results suggest that this reaction proceeds close to a concerted (S_N2-like) process.

The thick and thin filaments of muscle are made up primarily of myosin and actin. In muscle contraction, these proteins slide past each other through an interaction of the globular heads of myosin with monomer units of actin (*1, 2*). The binding of ATP to myosin reduces the affinity of myosin for actin, and the subsequent hydrolysis of ATP results in a metastable ternary complex myosin·ADP·Pi. The release of ADP and Pi is catalyzed by the rebinding of actin. Overall, the energy needed to drive the sequence of steps leading to the myosin/actin sliding motion is driven by the hydrolysis of ATP (cf. ref *3*); hence, there is considerable interest in understanding binding interactions and structure of the ATP binding site and the enzymic mechanism that catalyzes the hydrolysis process.

The soluble myosin head fragment, subfragment-1 or S1, can be isolated, and it contains both the ATPase and actin binding sites. Vanadate has been used extensively in the studies of enzyme-catalyzed phosphotransfer reactions since it not only demonstrates physical and chemical similarities with phosphate but also exhibits considerable plasticity in the formation of VO bonds with large variations of bond strengths and the readiness to add an additional fifth ligand. Because of these properties, vanadate has been shown to be a potent inhibitor of many enzymes that catalyze phosphotransfer (*4*−*7*). For myosin, vanadate inhibits myosin ATPase activity by forming an enzymic complex with MgADP (*8*). This complex is believed to mimic either the transition state of the hydrolysis reaction or the ADP·Pi intermediate (*9, 10*), and its structure and biochemical properties have been studied extensively.

Recently, a three-dimensional crystallographic structure of truncated myosin S1 and its complex with MgADP−vanadate has been determined (*10*). The vanadate moiety in the myosin S1·MgADP·Vi complex is trigonal bipyramidal, with three short equatorial V⋯O bonds and two long apical V−O bonds. One of the three equatorial V⋯O bonds interacts with a structural Mg^{2+} while each of the other two equatorial bonds are hydrogen bonded to protein residues. One of the vanadium apical V··O bonds is formed with oxygen of the β-phosphate of the ADP leaving group while the other is formed with a water molecule. The two apical V··O bonds are quite long, 2.09 and 2.27 Å, respectively, which suggest that the bonds are weak.

Raman difference spectroscopy (*11*) is well suited for the determination of high-resolution VO bond lengths and bond orders of vanadate complexes in enzymes (*12*−*15*), and the measurements report on solution complexes. In such studies,

† This work was supported by grants from the National Institutes of Health (GM35183 to R.H.C. and DK05195 to R.G.Y.).

‡ City College of the City University of New York.

§ Albert Einstein College of Medicine.

|| Washington State University.

S0006-2960(98)00556-X CCC: $15.00
Published on Web 07/16/1998

the Raman spectrum of the protein−vanadate complex is measured as is that of the protein alone. The difference spectrum between these two spectra contains bands arising from the vanadate group. The vanadate bands dominate the difference spectrum due to their intrinsic large intensity and because most of the protein background spectrum subtracts out (*12*−*14*). Definitive band assignments are accomplished by studies of isotopic ^{18}O-labeled vanadates. The bond lengths and bond orders of the nonbridging V⋯O bonds are determined from empirical correlations relating the vibrational stretch frequencies to these quantities (*15, 16*). The absolute accuracy is very high. The error in these relationships is estimated to be within ±0.04 vu and ±0.004 Å for bond orders and bond lengths, respectively. From these values for the nonbridging V⋯O bonds, the total bond order of the apical V−O bonds in the bound vanadate moiety is determined. Moreover, the geometry of the VO bonds can also be ascertained from the vibrational frequencies.

We report here on the Raman difference measurements of the nonbridging V⋯O stretch mode frequencies of the myosin S1·MgADP·Vi complex and model compounds in solution. Large changes of the vanadate Raman spectra were observed when vanadate binds to the complex. Employing both the previous empirical relationships between bond orders/lengths and frequencies as well as vibrational analysis from ab initio calculations, the spectral changes can be explained by a small decrease of the nonbridging V⋯O bond orders of the ADP−Vi moiety in the myosin S1·MgADP·Vi complex and by an increase of the angle between adjacent nonbridging V⋯O bonds. Our results show that formation of a fifth long V··O bond with a structural water molecule, opposite to the bridging V−OR bond, can induce the V⋯O bond order change and geometry change of the three nonbridging V⋯O bonds determined from the stretching modes frequency shifts. Implications of these structural results on the reaction mechanism of ATP hydrolysis catalyzed by myosin are discussed.

MATERIAL AND METHODS

Enzyme Preparations. Myosin was prepared from rabbit leg and back muscles as described by Wagner and Yount (*17*). Chymotryptic S1 was prepared by a modification of the method of Okamoto and Sekine (*18*) as previously described (*19*). The S1·MgADP·Vi complex was formed by incubation of S1 with $MgCl_2$, ADP, and Vi as previously described (*19*). The S1·MgADP·AlF_4 complex was formed by incubation of S1 with 2 mM $MgCl_2$, 0.2 mM ADP, 5 mM NaF, and 0.1 mM $AlCl_3$ for 30 min at 25 °C. The complexes were purified by precipitation with 2 volumes of saturated ammonium sulfate and centrifuged, and the pellets were resuspended in minimal S1 buffer (50 mM Tris, 100 mM KCl, 0.01% NaN_3, pH 8.0 at 4 °C) and passed through a centrifugal gel filtration column as previously described (*19*). The complexes were concentrated using Centricon 50 concentrators (Amicon). Since the oxygens on vanadate nonbridging V⋯O bonds exchange with solvent water rapidly, ^{18}O labeling of these oxygens can be achieved by exchanging the above samples by several cycles of dilution with S1 buffer prepared with ^{18}O water (>95%, Cambridge Isotope Laboratories) and reconcentration using the Centricon 50.

Raman Spectroscopy. The difference Raman spectrometer used in the experiment has been described in detail previously (*11, 13, 14, 20*). The Raman spectra were obtained with 100 mW at 514.5 nm from an argon ion laser beam. A half-wave retarder was used to orient the polarization of the incident light either parallel or perpendicular to the entrance slit of the spectrometer. The symmetry of a vibrational mode was assessed in terms of the ratio of Raman intensities obtained with the excitation beam in the perpendicular and parallel configurations relative to the spectrometer entrance slit. In this optical arrangement, the intensity ratios are 6/7 for an asymmetric mode and <6/7 for a symmetric mode (*21*). This geometry, rather than the more common one that determines the "depolarization ratio", was employed to maximize signal throughput. The polarization response of the spectrometer was calibrated by measurements of the toluene spectrum, where the symmetry of the various bands is known. The resolution of the spectrometer was set at 8 cm^{-1} with band positions accurate to ±3 cm^{-1}.

Ab Initio Calculations. Cartesian force constants and the Raman polarization tensor of an isolated dianionic vanadate or methylvanadate were calculated by Gaussian 94 program (*22*) at the HF/3-21g* level. The Cartesian force field was converted to the internal force field by the program REDONG (Allouche, QCPE) and subsequently "scaled" (by a set of scaling factors) so that the calculated vibrational frequencies and isotopic shifts of the vanadate derivatives were in good agreement with those that were observed. The Raman intensities (and their dependencies on incident light polarization) of the new vibrational modes were also calculated, by using the Raman polarization tensor obtained in the initial ab initio calculations and the new normal-mode eigenvectors obtained by the scaled force field. These quantities were then compared with the experimental spectra to evaluate the scaling factors. Once a set of satisfactory scaling factors is obtained, calculations on a series of models of the vanadate moiety simulating S1·MgADP·Vi complex were then performed by Gaussian 94. The calculated force fields from these model vanadate complexes were scaled, using the scaling factors determined from the calculations on the isolated model complex, to produce the vibrational modes, Raman intensities, and polarization dependencies.

RESULTS

Figure 1A shows the Raman spectrum of vanadate in aqueous solution at pH 10. The spectrum using parallel polarized incident laser light is plotted on top of the perpendicularly polarized spectrum. Figure 1B shows a similar spectrum of the same vanadate sample prepared in 95% ^{18}O water. At pH 10, vanadate is dianionic and therefore contains one V−OH bond and three nonbridging V⋯O bonds with similar bond lengths. The stretch motions of these three bonds are strongly coupled to form a symmetric V⋯O stretch mode and a doubly degenerate asymmetric V⋯O stretch. The most prominent Raman band in $H_2{}^{16}O$ water is the symmetric mode, which lies at 870 cm^{-1}, and the much weaker asymmetric mode lies at virtually the same place, 869 cm^{-1} (Figure 1A). The symmetric mode dominates the parallel polarized Raman spectrum but becomes the minor band in the Raman spectrum when the perpendicularly polarized laser light is used for Raman excitation. This occurs because the perpendicular/parallel intensity ratio

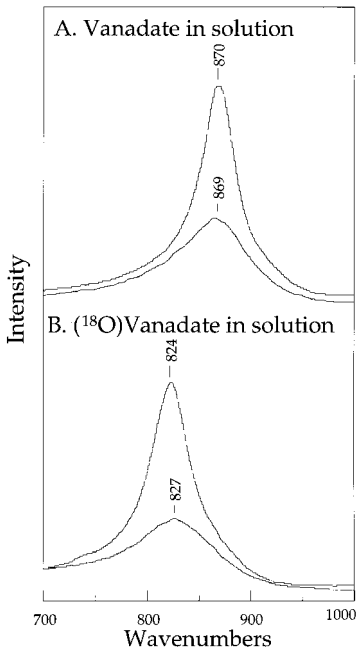

FIGURE 1: (A) Raman spectrum of 100 mM HVO_4^{2-} at pH 10. The top curve is the parallel polarized spectrum with the Raman excitation laser beam parallel to the spectrometer's entrance slit plane, while the bottom graph is the perpendicular spectrum (excitation laser beam perpendicular to the spectrometer's entrance slit plane). (B) Same as part A except prepared in ^{18}O water; 100 mW of the 514.5 nm laser line from an argon ion laser was used to excite the Raman scattering, and the spectral resolution was 8 cm^{-1}.

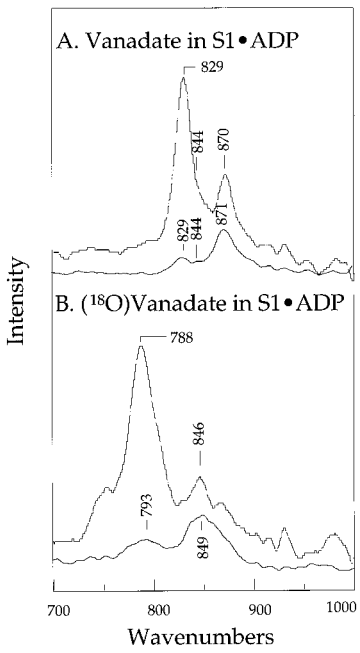

FIGURE 2: (A) Raman difference spectrum between the myosin S1·MgADP·Vi complex and the myosin S1·MgADP·AlF_4- complex, pH 8. The top curve is the parallel polarized spectrum with the Raman excitation laser beam parallel to the spectrometer's entrance slit plane, while the bottom graph is the perpendicular spectrum (excitation laser beam perpendicular to the spectrometer's entrance slit plane). (B) Same as A except prepared in ^{18}O water; 100 mW of the 514.5 nm laser line from an argon ion laser was used to excite the Raman scattering, and the spectral resolution was 8 cm^{-1}. The temperature of the sample was maintained at 4 °C during the Raman measurements.

of the symmetric mode is small (less than 6/7) while that of an asymmetric stretch mode is 6/7 under our experimental conditions (see Material and Methods). The assignment of these bands to V⋯O stretch modes was confirmed by ^{18}O labeling of the dianionic vanadate; the frequencies of these two modes shift down by about 45 cm^{-1} (Figure 1B). The relative positions of the symmetric and asymmetric modes are important for structural determinations, as will be shown below. The Raman spectra of another vanadate model compound, methylvanadate monoester dianion, shows the same symmetric and asymmetric V⋯O stretch frequencies at 870 cm^{-1} in solution (*12*). Therefore, the frequencies V⋯O stretch modes due to the three nonbridging V⋯O bonds in dianionic vanadate derivatives are little affected by different R groups of the bridging $RO-VO_3^{2-}$ bond formed with vanadium, as long as this bond is formed with an oxygen atom.

Raman difference spectra between the S1·MgADP·Vi complex and S1 alone were also measured (data not shown). However, because the binding of MgADP·Vi induced significant protein structural changes and altered frequencies, this difference spectrum contains many protein Raman bands in addition to the Raman bands from the MgADP−Vi moiety. The result of this is to obscure the assignment of the weaker Raman bands of the vanadate moiety, such as the asymmetric V⋯O stretch mode. Previous X-ray crystallographic studies have shown that the protein conformations are similar in the myosin S1·MgADP·Vi and myosin S1·MgADP·AlF_4 complexes (*10, 23*). Thus, the Raman difference spectrum between these two complexes, which shows substantially less contributions from protein, was obtained and is shown in Figure 2A. Two clearly resolved Raman bands in the spectral region between 600 and 1000 cm^{-1} can be assigned to the V⋯O stretch modes of the bound vanadate moiety on the basis of their shift upon ^{18}O labeling of the nonbridging V⋯O bonds in S1·MgADP·Vi complex (Figure 2B). In addition, a nearly resolved band at 844 cm^{-1} (best seen in the perpendicularly polarized spectrum of Figure 2B) can also be assigned to a V⋯O stretch. On the basis of the relative intensities of the band at 870 and 829 cm^{-1} and on the changes in intensity they undergo for parallel versus perpendicular polarized incident laser light (Figure 2B), these bands are assigned to "nearly" asymmetric and symmetric V⋯O stretch modes, respectively. The presence of a third band at 844 cm^{-1}, which has an intensity ratio intermediate between a symmetric (perpendicular to parallel polarized intensity ratio near 0) and an asymmetric mode (ratio of 6/7), suggests that the C_{3v} symmetry of the vanadate dianion in solution has been broken when vanadate binds to the S1·MgADP subfragment. That the symmetry of the three V⋯O bonds in the complex is somewhat altered from a nearly perfect C_{3v} symmetry in solution is also consistent with the observation that the intensity ratio of the "symmetric" V⋯O stretch mode in the complex at 829 cm^{-1} using perpendicular polarized laser light compared to parallel polarized light is significantly larger than 0, as shown by the finite intensity of the band at 829 cm^{-1} in the perpendicularly polarized spectrum (Figure 2A).

Since the binding site of the S1 subfragment has been designed to bind dianionic γ-phosphate of ATP, it is expected that the ionic state of vanadate in the binding pocket is also dianionic. The monoanion, the dominant form for vanadate at the pH 8 conditions of our experiments (pK_a of 8.5; ref

12), shows a symmetric Raman V⋯O band in solution at about 940 cm^{-1}, much higher than the observed bands of the bound vanadate. This ~100 cm^{-1} difference of the nonbridging V⋯O bonds would imply a large reduction of V⋯O bond order and a large concomitant increase in the bond order of the bridging V−O bonds of the vanadate in the S1·MgADP·Vi complex (see below). The predicted bond order of the bridging V−O bonds in the complex is much too large to be consistent with the crystallographic results. In addition, monoanionic vanadate can yield only two Raman bands of V⋯O character while three are observed. We conclude that the ionic state of the bound vanadate is dianionic.

It has been shown that the S1·MgADP·Vi complex undergoes a photoreaction when it is illuminated with UV light (*19*, *24*), resulting in the release of ADP and vanadate from the complex. We did not observe significant vanadate release from the S1·MgADP·Vi complex during our Raman experiment since such release would result in loss of intensity of the 829 and 870 cm^{-1} bands characteristic of the bound vanadate ion and the concomitant gain of signal in positions characteristic of free vanadate found in aqueous solution at pH 8 (see e.g., refs *12* and *25*). No degradation of the 829 and 870 cm^{-1} bands was observed. Apparently, our Raman excitation laser wavelength, 514.5 nm, is far removed from the absorption of the S1·MgADP·Vi complex so that little photoreaction occurred. On the other hand, similar experiments performed on the S1·CoADP·Vi complex did result in a slow sample degradation during the Raman measurement, as shown by a significant intensity reduction of the 829 cm^{-1} band (data not shown).

Bond Length/Bond Strength/Vibrational Frequency Relationships and the O⋯V⋯O Angle. Accurate structural information about bonding in both metal and nonmetal oxides often can be obtained from vibrational spectroscopy by using two types of empirical relationships. The following equations hold for vanadates (see refs *16* and *15*):

$$s_{VO} = (r_{VO}/1.791)^{-5.1} \quad (1)$$

and

$$s_{VO} = [0.2912 \ln(21349/\nu)]^{-5.1} \quad (2)$$

where s_{VO} is the valence bond order given in terms of valence units, vu, and defined such that the sum, $\sum s$, of all bonds is the valence of the central vanadium atom, which is equal to 5 (*26*, *27*); r_{VO} is the length of the VO bond given in Å; and ν, given in cm^{-1}, is the geometric mean of the observed nonbridging V⋯O stretches $[(\nu + d\nu)/(d + 1)]^{1/2}$ (ν_s is the symmetric stretch, ν_a is the asymmetric stretch, and $d = 2$ is the degeneracy of the asymmetric modes). The absolute error in these relationships in determining bond lengths and bond orders from frequency measurements is estimated to be within ±0.04 vu and ±0.004 Å for bond orders and bond lengths, respectively, and more accurate for determining changes (*15*).

For the vanadate solution model, $\nu = 869.3$ cm^{-1} from $\nu_s = 870$ cm^{-1} and $\nu_a = 869$ cm^{-1}, which yields a bond order of 1.430 vu and a bond length of 1.669 Å for each of the three nonbridging V⋯O bonds using eqs 1 and 2. For the V⋯O bonds in the S1 subfragment bound vanadate, the shift to lower frequency translates to a somewhat higher bond order and lower bond length for the three bonds. From eqs 1 and 2, the three frequencies at 829, 844, and 870 cm^{-1} yield bond orders of 1.327, 1.365, and 1.433 vu and bond lengths of 1.694, 1.685, and 1.669 Å, respectively, of the three nonbridging V⋯O bonds.

Analytical expressions relating the measured frequencies to the force constants and geometry of the V⋯O bonds have been obtained (*15*). To a high degree of accuracy, only three parameters are important to determine the symmetric (ν_s) and asymmetric (ν_a) V⋯O stretch frequencies in addition to the mass of the atoms: the V⋯O stretch force constant, Fs, the V⋯O stretch/stretch coupling force constant, Css, and the O⋯V⋯O angle, ϑ. According to the analytical expressions for ν_s and ν_a, a change of Fs results in a change of both ν_s and ν_a in the same direction, as expected. On the other hand, a change of the angle ϑ or Css results in opposite changes of ν_s and ν_a so that the frequency difference between these two stretch modes changes. When $\vartheta > 90°$, an increase of the angle results in a ν_s decrease but a ν_a increase. In short, the geometry change of the VO_3^{2-} moiety can be determined on the basis of changes in the V⋯O stretch frequencies, ν_s and ν_a. This is because the changes of the force constant Fs (thus the bond length) can be determined from the change in ν, which is relatively insensitive to geometry changes, and the change of the angle can be determined by the change of the difference between ν_s and ν_a, provided that some knowledge about the Fs/Css ratio is known (e.g., unchanged as suggested by ab initio calculations). Thus, the Raman spectral changes of the vanadate upon forming the S1·MgADP·Vi complex can be explained by the following physical changes of the VO_3^{2-} moiety: an increase of the angle between any two V⋯O bonds (hence VO_3^{2-} becomes more planar) with a concomitant small decrease in the average V⋯O stretch force constant Fs (hence, a small increase of the V⋯O bond lengths).

The increase of the angle ϑ upon vanadate binding to the S1·MgADP·Vi complex can be estimated quantitatively using the analytical expressions for ν_s and ν_a of dianionic vanadate (eqs 7 and 8 in ref *15*). For dianionic vanadate in solution, the angle ϑ can be estimated by ab initio calculations ($\vartheta = 111°$, see below), Fs can be determined directly from the fundamental stretch frequency as pointed out above, and Fs/Css can be determined from the difference between ν_s and ν_a (Fs/Css = 10.5). Since the Fs/Css ratio does not change much according to ab initio calculations, ϑ can be calculated exactly for a VO_3^{2-} moiety having C_{3v} symmetry. However, it is clear from the results that the symmetry has been broken in the protein complex (two asymmetric modes are observed at different frequencies), so that the analytical formulas cannot be applied strictly. As an approximation, assuming the C_{3v} symmetry and taking $\nu_s = 870$ cm^{-1} and $\nu_a = 829$ cm^{-1} in the S1·MgADP·Vi complex and assuming that the value of the Fs/Css ratio is the same as in solution, then it is calculated that $\vartheta = 119°$ (a value of 120° is a planar VO_3^{2-} moiety). Since another V⋯O stretch mode was observed at 844 cm^{-1} (see results), we expect the average angle ϑ between pairs of V⋯O bonds to be somewhat smaller.

Ab Initio Vibrational Analysis of Dianionic Vanadate. Quantum mechanical ab initio calculations were performed to model the vanadate binding and to assess the interactions

assumed to take place at the binding site. It is well-known that chemical bond lengths, especially those bonds which contain oxygen, are underestimated by ab initio methods at the Hatree-Fock level compared with the observed values (by about 20%). However, the overestimation of the calculated spectral differences compared to experimentally determined values between different conformations of a given molecule tends to remain constant (*28*−*30*). Thus a scaling procedure can be adopted to reduce the errors in the absolute frequencies calculated by ab initio methods but to retain its predicting value on the spectral change of the molecule when the conformation of the molecule is changed by external perturbation.

The model system used in our ab initio calculations is methylvanadate dianion, and the simulated Raman spectra of vanadate dianion in the V⋯O stretch mode region based on the ab initio calculations and empirical scaling of the force field are presented in Figure 3A. The results of geometry optimizations indicate that the bridging V−O bond is not collinear with the bridging O−C(H) bond at equilibrium. One of the nonbridging V⋯O bonds is longer compared to the other two, so that the C_{3v} symmetry expected for the three nonbridging V⋯O bonds is slightly broken. Three nonbridging V⋯O stretch modes, at 869, 865, and 851 cm^{-1}, respectively, are predicted after application of the scaling procedure described above (Figure 3A). Thus the calculations do not take into account fast rotation of the methyl group about the bridging bond, which would result in an average equal environment for each of the three nonbridging V⋯O bonds. However, this result of the calculations is not important for our purposes. For a VO_3^{2-} group with perfect C_{3v} symmetry, the displacements of the three oxygens in the symmetric stretch mode are in phase and with the same magnitude. One asymmetric mode has an eigenfunction where one oxygen has 0 displacement while the other two nonbridging oxygens are out of phase with the same magnitude. In the second asymmetric mode, the displacement of one oxygen is out of phase with the other two and its magnitude is twice as large. Although the VO_3^{2-} group in our solution model compound does not have a perfect C_{3v} symmetry, the resultant stretch modes can still be identified on the basis of the above classification. The 869 cm^{-1} mode corresponds to the symmetric stretch mode, with the perpendicular to parallel polarization intensity ratio very close to 0 (Figure 3A). The character of the 865 cm^{-1} mode is the quite close to the asymmetric modes for VO_3^{2-} with C_{3v} symmetry since the two (shorter) V⋯O bonds have out of phase displacements and there is no displacement of the third oxygen. The mode also has a depolarization ratio characteristic of an asymmetric mode. Likewise the 851 cm^{-1} mode resembles the second asymmetric mode discussed above closely and has an intermediate polarization ratio (0.12). Calculations were also performed on methyl vanadate where the nonbridging oxygens were replaced by ^{18}O. The 869 cm^{-1} band moves to 816 cm^{-1}, the 856 cm^{-1} band to 835 cm^{-1}, and the 851 cm^{-1} band to 830 cm^{-1}. For presentation, all bands were assigned a bandwidth that matches the experimentally determined bandwidth; the bandwidth does not come out of the calculations. It can be seen that the agreement between the measured (Figure 1A) and calculated Raman spectra (Figure 3A) is reasonable as are the ^{18}O-induced shifts. Thus the scaling factors obtained here were used in subsequent Raman spectrum calculations of vanadate complexes simulating that found in S1·MgADP·Vi.

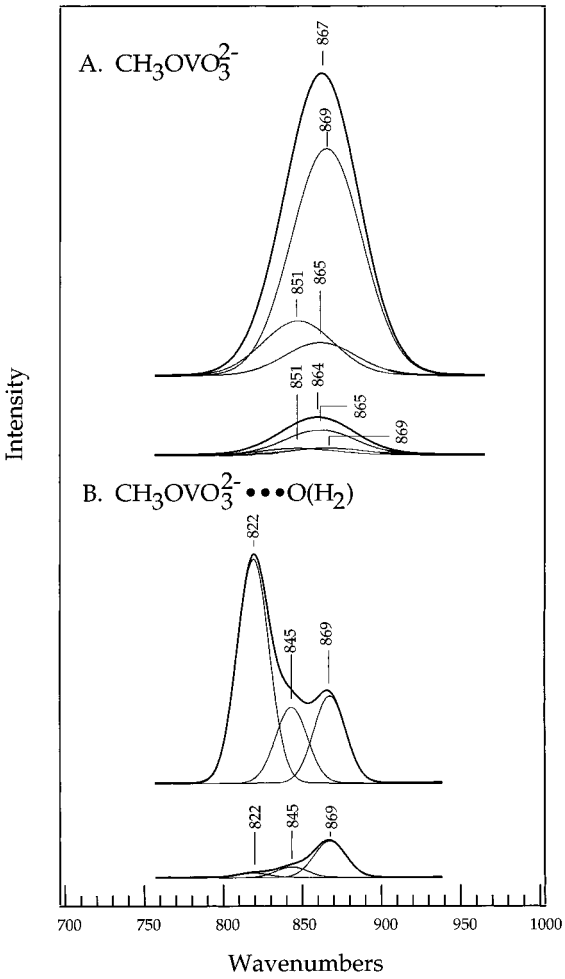

FIGURE 3: (A) Calculated Raman spectrum of dianionic methylvanadate from ab initio calculations as described in the text. The top curve is the simulated parallel polarized spectrum, and the bottom curve is the perpendicular polarized spectrum. The individual Raman bands are simulated by a guassian function, and the bandwidth is set to 22 cm^{-1}. The curves identified at 867 cm^{-1} (top) and at 864 cm^{-1} (bottom) are the envelop (observable) spectra arising from the three bands. (B) Calculated Raman spectrum of dianionic methylvanadate complexed with a water molecule at a water oxygen−vanadium distance of 2.5 Å. The top curve is the simulated parallel polarized spectrum, and the bottom curve is the perpendicular polarized spectrum. The Raman bands are simulated by a guassian function, and the bandwidth is set to 10 cm^{-1}. The curves identified at 822 cm^{-1} (top) and 869 cm^{-1} (bottom) are the envelop (observable) spectra arising from the three bands.

To simulate the vanadate moiety in the S1·MgADP·Vi complex, a water molecule opposite the bridging V−O bond of methylvanadate dianion was placed at various distances. The geometry of the complex, with the vanadium-water−oxygen distance fixed at various lengths, was optimized with the 3-21g* basis set. The force field and Raman polarization intensity ratios of normal modes were obtained in subsequent frequency calculations. Using the scaling factors obtained in the solution model calculations, the scaled force field and resulting frequencies were then calculated. Table 1 shows the results of calculations on several model complexes with V−O(H_2) distance ranging from 2.25 to 4.0 Å (and at infinity, e.g., no interaction). It was found that for a water

Table 1. The O···V···O Angle, $CH_3O-VO_3^{2-}$ Bond Length, and V···O Bond Length as a Function of Water−Methylvanadate Distance in the Model of the Active Site of Myosin S1·MgADP Vi Complex from ab Initio Calculations

CH_3OVO_3···OH_2 bond length (Å)	O···V···O angle (degrees)	$CH_3O-VO_3^{2-}$ bond length (Å)	V···O bond length (average, Å)
$CH_3OVO_3^{2-}$	111.2	1.907	1.636
4.0	112.1	1.914	1.636
3.5	112.4	1.915	1.637
3.0	113.3	1.917	1.639
2.75	114.3	1.918	1.641
2.5	115.6	1.922	1.645
2.25	117.2	1.931	1.651

oxygen−vanadium distance of about 2.5 Å the calculated Raman spectrum of the nonbridging V···O bonds shows a pattern quite similar to that observed in the Raman spectrum of the S1·MgADP·Vi complex. The Raman spectra calculated from this 2.5 Å model complex are presented in Figure 3B. The 822 cm^{-1} band moves to 780 cm^{-1} upon ^{18}O replacement of the nonbridging V···O oxygens, the 869 cm^{-1} band to 839 cm^{-1}, and the 845 cm^{-1} to 816 cm^{-1}. As can be seen, the calculated pattern of bands and their intensity ratios between parallel and perpendicular polarizations, and shifts upon ^{18}O substitution, are in quite good agreement with the observed spectra (compare Figures 2A and 3B). The crystallographic study of the S1·MgADP·Vi complex places the V−O(H_2) distance at 2.27 Å (*10*), in very good agreement with the present results.

The results in Table 1 show that to push a water molecule toward vanadium of the vanadate dianion along the bridging V−O bond from the vanadium end causes two general changes in the VO_3^{2-} geometry: the first is to increase the average V···O bond length; the second is an increase of the average bond angle between two V···O bonds, resulting in a more planar VO_3^{2-} moiety. For example, the average V···O bond length is about 0.009 Å longer in the 2.5 Å model complex than that in isolated vanadate while the average angle between two adjacent nonbridging V···O bonds is increased by about 4.4°, from 111.2° in isolated vanadate dianion to 115.6° in the 2.5 Å model complex.

A series of calculations was performed using hydroxyl (OH^-) rather than water as the attacking nucleophile. As expected, the presence of a full negative charge on the hydroxyl influenced the vanadate vibrational frequencies much more strongly than does the neutral (but polar) water for the same V−O distance. Essentially the same shifts in frequency were observed in the ab initio calculations at 3.0 Å for OH^- compared to the 2.5 Å water results. The results suggest that the attacking nucleophile at the S1 binding site, observed only as an oxygen in the X-ray results, is water rather than OH^-. It is possible, however, that a highly solvated or hydrogen-bonded hydroxyl, so that the hydroxyl charge is highly screened, could also account for the experimental results.

Test calculations on model compounds including a Mg^{2+} or Na^+ ion next to one of the nonbridging oxygens were not successful because the interaction between Mg^{2+} and vanadate moiety was greatly overestimated by ab initio methods. The results predict that the nonbridging V···O bond interacting with Mg^{2+} would be too greatly polarized (data not shown). Such effects are not observed in our Raman studies. Therefore, much more complex model systems, involving hydrogen bonding or ionic interactions on all three nonbridging V···O bonds and with the metal ions, are required to reproduce the observed Raman spectrum of vanadate moiety in the S1·MgADP·Vi complex if ions are to be included in the model complex.

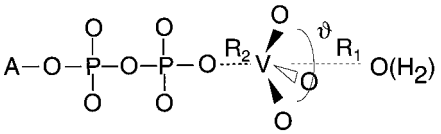

FIGURE 4: A schematic of ADP··Vi··O(H_2) at the S1 binding site, which defines the molecular coordinates used in the text to describe the reaction coordinate. For the trigonal bipyramidal transition-state structure believed to occur in phosphotransfer reactions (cf., ref *46*), the nonbridging P···O bonds are planar. The following conventions have been used to categorize the structure of the transition state: the bond order of R1 + R2 at the transition state is much smaller than the reactant states for a dissociative transition state and substantially larger than the bond order of the ground-state bridging P···O bond for an associative transition state. The bond order of the two axial bonds remains the same as that of the original PO bond for a synchronous reaction (S_N2-like). The bond orders, as defined by valence bond strength (see text), of the ground states for various bridging RO−PO_3^{2-} bonds are close to 1.

DISCUSSION

A number of structural conclusions can be made on the basis of our difference Raman spectroscopy studies of the S1·MgADP·Vi complex and of the empirical and ab initio vibrational analyses of the Raman data. Vibrational frequencies are determined by the force constants within chemical bonds and the geometry of the atoms that make up a molecule. Hence, vibrational frequencies report on bond orders, bond lengths, and geometry. Moreover, both the vanadate model compounds and the S1·MgADP·Vi complex can be studied as solution structures by Raman spectroscopy. Figure 4 shows a cartoon of the S1 binding site containing ADPO···VO_3^{2-}···O(H_2), and the relevant bond lengths and angles.

The vibrational results show that the ionic state of the bound vanadate is dianionic. The average bond order of the three nonbridging V···O bonds for vanadate in the protein complex is decreased by 0.05 vu compared to vanadate in aqueous solution, from 1.43 to 1.38 vu. This means that, although the ionic and hydrogen-bonding interactions between the nonbridging V···O bonds and Mg^{2+}/protein residues are well-coordinated in the S1·MgADP·Vi complex, the average strength of these interactions is just a bit stronger than for those between the nonbridging V···O bonds and counterion/water in aqueous solution. Stronger interactions would polarize the V···O bonds more by bringing about a proportional decrease in their bond orders. The average V···O bond length is correspondingly increased slightly to 1.683 Å in the S1·MgADP·Vi complex, which is 0.014 Å longer when compared to the solution value. The Brown and Wu paradigm (*27*) has it that the sum of the bond orders of all VO bonds in the S1·MgADP·Vi complex is equal to 5. Thus, the total bond order of the two apical bonds should be about 0.86 vu. Assuming the two apical bonds (R_1 and R_2, Figure 4) each have a bond order of 0.43 vu, this corresponds to two V−O bonds with average bond length of 2.10 Å each. As derived in the Results section, the relative positioning of the symmetric and asymmetric V···O stretch

modes confirms that the VO_3^{2-} constellation approaches a more planar conformation than that found in solution by a substantial amount. From the observed V···O stretch frequencies, it is calculated that the O···V···O bond angle in the S1·MgADP·Vi complex (ϑ in Figure 4) may increase by up to 8° relative to the solution model compound, approaching the value of 120° which corresponds to a planar VO_3^{2-} group.

The bond lengths determined from the present spectral results are close to, but not identical with, those obtained from crystallography (*10*). The three equatorial V···O bond lengths found herein, at 1.694, 1.685, and 1.669 Å, are on average about 0.02 Å longer than those found in the X-ray crystallographic studies at 1.67, 1.67, and 1.64 Å, while the average of the two V−O apical bonds is about 0.08 Å shorter. This discrepancy is larger than our error in determining bond lengths, ±0.004 Å (*15*). Recently, the spectra of the near-UV circular dichrosim of S1·MgADP·Vi in solution and of vanadate model compounds were reported (*31*). The protein spectrum resembles that of model octahedral coordinated vanadates rather than trigonal bipyramidal coordination. However, our vibrational results are in agreement with the X-ray results which find a trigonal bipyramidal coordination. We observe three Raman bands for the nonbridging V···O bonds in the S1·MgADP·Vi complex where four are expected for octahedral coordination. Moreover, the extra bond suggested for octahedral coordination would be expected to yield a much larger downshift in frequency for the V···O stretch frequencies than is observed.

The active site of S1 contains many groups that can interact with the vanadate group to bring about its change in geometry. The ab initio calculations show that the V···O bond orders and the O···V···O bond angle are quite sensitive to the distance between the vanadium atom and the oxygen of the attacking in-line H_2O water molecule at the binding site. The spectroscopic changes for the V···O stretch frequencies observed when vanadate binds to S1, which are large and are of an unusual nature, are well accounted for by placing the attacking water 2.5 Å from the vanadium atom (see Figure 4), in reasonable agreement with the 2.27 Å distance observed in the crystallographic studies (*10*). The ab initio analysis confirms that the average angle between two nonbridging V···O bonds increases as MgADP·Vi binds to S1, but by a slightly smaller amount than that given by the analytical expressions, by 4−5° from the solution value to reach $\vartheta = 116°$ in the complex. Larger changes of the bond angle, which can be induced either by forcing the apical water molecule closer to vanadate or by lengthening the second apical V−O bond in the model complexes, can be readily obtained, but this results in too large a frequency difference between symmetric and asymmetric nonbridging V···O stretch modes compared to that observed in the Raman experiments.

It is clear that there is a substantial interaction between the VO_3^{2-} group and the binding site water molecule. Our results suggest then that the ATPase active site of myosin is configured in such a way so as to hold the attacking nucleophile close enough and tight enough to the phosphorus atom of the γ-phosphate of bound ATP to cause a significant interaction between them and to facilitate catalysis. Indeed, it is clear that ATPase activity at the active site of myosin is brought about by attack of a water molecule on the γ-phosphorus atom (*32*−*34*), and such a positioning of the active site water molecule is certainly consistent with the structure and hydrogen bonding patterns found at the active site of S1 (*10*). We have recently observed the same type of interaction between bound GTP and the active site water in the GTPase active site of the c-Harvy-ras p21 protein based on vibrational spectroscopic studies, suggesting a similar enzymic mechanism for the two proteins (*35*).

The electronic nature of the transition-state structure in a phosphotransfer reaction can be categorized by whether it is dissociative (one where the bond breaking of the original ester P−O bond is almost complete before significant formation of the new P−O bond so that the sum of the apical bonds is decreased substantially compared to the original ester P−O bond), associative (wherein there is considerable bond formation between the attacking nucleophile and phosphorus before much bond breaking with the leaving group so that the summed PO bond order of the apical bonds is increased substantially), or concerted (S_N2-like). In the latter case, the summed PO bond strength of the apical bonds in the transition state remains unchanged compared to the ground-state ester bond, which is close to 1 for dianionic monoester phosphates (*15*). Phosphotransfer reactions involving monoester dianionic phosphate in aqueous solution are via a primarily dissociative pathway, with a metaphosphate-like transition state (ref *36*, and references therein). Here, the bond breaking of the original ester P−O bond is almost complete before significant formation of the new P−O bond, and the sum of the bond orders of the broken and new bonds is significantly less than 1. However, the mechanism(s) in enzymes is far from clear, and both associative and dissociative transition states have been proposed (see, e.g., refs *7*, *13*, and *37*−*44*).

Vanadate's ability to bind to phosphotransfer enzymes derives from its ability to increase its coordination sphere to five or six bonds and to readily form long bonds. In many systems such as myosin, vanadate binds very tightly to the enzymic binding site, which satisfies the criterion that a transition-state analogue must bind much tighter than the substrate of the enzyme. In addition to binding tightly, vanadate forms the expected pentacoordinated geometry of the transition state in the S1·MgADP·Vi complex. The present studies are very sensitive to the bond orders (and bond lengths) of the vanadate moiety and to changes in bond orders when it forms the protein complex. At the level of our accuracy, which is unprecedented, it is not clear to what degree vanadate acts as a transition-state analogue for the enzyme phosphotransfer reaction in terms of the bond orders of the complex (as opposed to geometry) and, hence, to what degree its structure mimics the nature of the distribution of electrons in the transition state. In what follows, we assume that vanadate is distorted toward the transition state when it binds to S1·ADP, recognizing that a determination of a transition-state structure is difficult and requires a variety of techniques, such as kinetic isotope measurements. We focus on the *changes* in bond orders that occur upon binding in our analysis since the bond order of the ester bridging bond in dianionic vanadates, about 0.7 vu, is considerably different than that for phosphates. In fact, in one system, RNase A, when the changes in bond orders in the transition state relative to the phosphate ground state determined by ^{18}O kinetic isotope effects (*45*) were compared to the changes

in the bond orders of a protein vanadate complex, a quantitative agreement was found (*14*).

With this caveat, our results have shown that the total bond order of the three nonbridging V···O bonds in the S1·MgADP·Vi complex relative to that found in the model complex in solution is reduced by about 0.16 vu. Thus, the sum of the axial bond order is increased by 0.16 vu in the S1·MgADP·Vi complex compared with the solution model, provided that the loss in bond order of the nonbridging V···O bonds is transferred to the two axial VO bonds involving the entering and leaving groups (an excellent approximation for phosphates and vanadates). Hence, we would conclude from the observed rather small increase of the total apical bond order that the reaction mechanism is essentially concerted (S_N2-like). Taking the analogy further, the 0.16 vu relative increase would imply a small associative character to the transition state.

REFERENCES

1. Huxley, A. F., and Hanson, J. (1954) *Nature 173*, 973−976.
2. Huxley, A. F., and Niedergerke, R. (1954) *Nature 173*, 971−973.
3. Fisher, A. J., Smith, C. A., Thoden, J., Smith, R., Sutoh, K., Holden, H. M., and Rayment, I. (1995) *Biophys. J. 68*, 19s−28s.
4. Gresser, M. J., and Tracey, A. S. (1990) in *Vanadium in Biological Systems* (Chasteen, N. D. E., Ed.) Kluwer Academic Publishers, The Netherlands.
5. Crans, D. C., Felty, R. A., and Miller, M. M. (1991) *J. Am. Chem. Soc. 113*, 265−269.
6. Crans, D. C., and Shin, P. K. (1994) *J. Am. Chem. Soc. 116*, 1305−1315.
7. Zhang, M., Zhou, M., Van Etten, R. L., and Stauffacher, C. (1997) *Biochemistry 36*, 15−23.
8. Goodno, C. C. (1979) *Proc. Natl. Acad. Sci. U.S.A. 76*, 2620−2624.
9. Goodno, C. C., and Taylor, E. W. (1982) *Proc. Natl. Acad. Sci. U.S.A. 79*, 21−25.
10. Smith, C., and Rayment, I. (1996) *Biochemistry 35*, 5404−5417.
11. Callender, R., and Deng, H. (1994) *Annu. Rev. Biophys. Biomol. Struct. 23*, 215−245.
12. Ray, J. W. J., Burgner, I. J. W., Deng, H., and Callender, R. (1993) *Biochemistry 32*, 12977−12983.
13. Deng, H., Ray, W. J. B., John W., and Callender, R. (1993) *Biochemistry 32*, 12984−12992.
14. Deng, H., Burgner, J. W., and Callender, R. H. (1998) *J. Am. Chem. Soc. 120*, 4717−4722.
15. Deng, H., Wang, J., Callender, R., and Ray, W. J. (1998) *J. Phys. Chem. 102*, 3617−3623.
16. Hardcastle, F. D., and Wachs, I. E. (1991) *J. Phys. Chem. 95*, 5031−5041.
17. Wagner, P. D., and Yount, R. G. (1975) *Biochemistry 14*, 1900−1907.
18. Okamoto, Y., and Sekine, T. (1985) *J. Biochem. (Tokyo) 98*, 1143−1145.
19. Grammer, J. C., Cremo, C. R., and Yount, R. G. (1988) *Biochemistry 27*, 8408−8415.
20. Yue, K. T., Deng, H., and Callender, R. (1989) *J. Raman Spectrosc. 20*, 541−546.
21. Wilson, E. B. J., Decius, J. C., and Cross, P. C. (1955) *Molecular Vibrations*, Mcgraw-Hill, New York.
22. Frisch, M. J., Trucks, G. W., Head-Gordon, M., Gill, P. M. W., Wong, M. W., Foresman, J. B., Johnson, B. G., Schlegel, H. B., Robb, M. A., Replogle, E. S., Gomperts, R., Andres, J. L., Raghavachari, K., Binkley, J. S., Gonzalez, C., Martin, R. L., Fox, D. J., Defrees, D. J., Baker, J., Stewart, J. J. P., and Pople, J. A. (1994) *Gaussian 94, Revision D*, Gaussian, Inc., Pittsburgh, PA.
23. Fisher, A. J., Smith, C. A., Thoden, J. B., Smith, R., Sutoh, K., Holden, H. M., and Rayment, I. (1995) *Biochemistry 34*, 8960−8972.
24. Cremo, C. R., Grammer, J. C., and Yount, R. G. (1988) *Biochemistry 27*, 8415−8420.
25. Ray, W. J., Crans, D. C., Zheng, J., Burgner, J. W., Deng, H., and Mahroof-Tahir, M. (1995) *J. Am. Chem. Soc. 117*, 6015−6026.
26. Brown, I. D. (1992) *Acta Crystallogr. B48*, 553−572.
27. Brown, I. D., and Wu, K. K. (1976) *Acta Crystallogr. B32*, 1957−1959.
28. Deng, H., Chan, A. Y., Bagdassarian, C. K., Estupinan, B., Ganem, B., Callender, R. H., and Schramm, V. L. (1996) *Biochemistry 35*, 6037−6047.
29. Deng, H., Huang, L., Groesbeek, M., Lugtenburg, J., and Callender, R. H. (1994) *J. Phys. Chem. 98*, 4776−4779.
30. Deng, H., Burgner, J., and Callender, R. (1992) *J. Am. Chem. Soc. 114*, 7997−8003.
31. Ajtai, K., Dai, F., Park, S., Zayas, C. R., Peyser, Y. M., Muhlrad, A., and Burghardt, T. P. (1998) *Biophys. Chem. 71*, 205−220.
32. Dale, M. P., and Hackney, D. D. (1987) *Biochemistry 26*, 8365−8372.
33. Sleep, J. A., Hackney, D. D., and Boyer, P. D. (1980) *J. Biol. Chem. 255*, 4094−4099.
34. Webb, M. R., and Trentham, D. R. (1981) *J. Biol. Chem. 256*, 10910−10916.
35. Wang, J. H., Xiao, D. G., Deng, H., Webb, M. R., and Callender, R. (1998) *Biochemistry* (in press).
36. Herschlag, D., and Jencks, W. P. (1990) *Biochemistry 29*, 5172−5179.
37. Weiss, P. M., and Cleland, W. W. (1989) *J. Am. Chem. Soc. 111*, 1928−1929.
38. Jones, J. P., Weiss, P. M., and Cleland, W. W. (1991) *Biochemistry 30*, 3634−3639.
39. Hengge, A. C., Sowa, G. A., Wu, L., and Zhang, Z.-Y. (1995) *Biochemistry 34*, 13982−13987.
40. Hollfelder, F., and Herschlag, D. (1995) *Biochemistry 34*, 12255−12264.
41. Zhao, Y., and Zhang, Z.-Y. (1996) *Biochemistry 35*, 11797−11804.
42. Hengge, A. C., Denu, J. M., and Dixon, J. E. (1996) *Biochemistry 35*, 7084−7092.
43. Schweins, T., and Warshel, A. (1996) *Biochemistry 35*, 14232−14243.
44. Hengge, A. C., Zhao, Y., Wu, L., and Zhang, Z.-Y. (1997) *Biochemistry 36*, 7928−7936.
45. Sowa, G. A., Hengge, A. C., and Cleland, W. W. (1997) *J. Am. Chem. Soc. 119*, 2319−2320.
46. Mildvan, A. S. (1997) *Proteins: Struct. Funct. Genet. 29*, 401−416.

BI980556N